

Vítor Paixão Fernandes, Thiago Rosado de Paula, Rodrigo Costa do Nascimento, Roberto Gil Annes da Silva & Luiz Carlos Sandoval Góes

Technological Institute of Aeronautics - ITA, 12228-900, São José dos Campos, Brasil

Abstract

This article expands upon the analysis conducted in a flight campaign involving a flexible wing UAV with a 4m wingspan and an aspect ratio of 18.9, powered by electric propulsion. The UAV is equipped with a data acquisition system designed to explore the effects of flexibility. The initial phase of the campaign involved flight evaluations aimed at assessing the behavior of the system, particularly in terms of data acquisition. Data compatibility tests were examined using the Flight Path Reconstruction (FPR) technique and the Output Error Method (OEM). The outcomes of the FPR analysis indicate the consistency of the recorded data. The evaluation of biases, scale factors, and time delays using the FPR method successfully established correlations between the recorded data, with notable exceptions in the case of airspeed and angle of attack, which exhibited discrepancies in fitting with classic rigid body kinematics. In this work, the longitudinal FPR using OEM is augmented by incorporating the flexible aircraft dynamic model to provide a more accurate representation of the aircraft, accounting for flexibility effects. In the execution of the FPR, the state variables of the aircraft model, obtained by the integration of the kinematic expression and sensor-gathered data, were expanded by the addition of the structural dynamics. This modification has enabled the computation of α and β values at the vane positions, accounting for structural dynamics effects, and also evaluating accelerations at the wingtips. Synthetic data obtained from an aircraft simulation model were used to evaluate the FPR for the flexible aircraft, and the results have shown that this method can lead to good results when the aircraft model is available. The rigid and flexible FPR were applied to flight-recorded data, and the results obtained with the flexible FPR have not led to enhancements as seen in the simulated data, which indicates that further refinements must be made in the experimental procedures, and evaluations on the structural model and aircraft sensors must be conducted. In conclusion, the method can be used to evaluate additional information beyond the classic FPR developed solely relying on general rigid body kinematics.

Keywords: FPR, Flexible Aircraft, UAV, Flight Dynamics, Identification.

1. Introduction

Having a representative model is crucial in the aeronautic industry, and one way of enhancing model accuracy using real flight data is the system identification technique. This technique relies on gathered data, adequate physical models, correct experimental procedures, and a suitable data processing method. The data applied to the procedure must be corrected for biases, delays, and misalignment of sensors, among other possible negative influences. The Flight Path Reconstruction (FPR) is one way of achieving correction factors and can be used to validate the gathered sensor data according to the mathematical model of the system, while also allowing the correction of systematic errors, being used as the first step in the system identification procedure [1].

The FPR has been applied to system identification in flexible aircraft by [2] and [3], using the assumption that the kinematic equations of a rigid-body aircraft would be valid, as the flight data instrumentation needed for the FPR development would not be influenced by the aircraft structural dynamics.

Based on the work developed by [2] and [3], a UAV called EOLO was used as a test platform to develop studies related to flexible aircraft dynamics and system identification in the time domain at the Aeronautics Institute of Technology (ITA). Following the Quad-M methodology [1], flight test campaigns were developed, including all the steps from which the method derives its name: maneuver, measurements, method, and model. Planned maneuvers developed by [4] were used as inputs, being executed automatically using a strategy described by [5]. However, the rigid body kinematic model used in the FPR has not been successful in achieving a good fit with the gathered data for the angle of attack (α) , whose response is influenced by the structural dynamics of the flexible aircraft wing on which the vane sensor is mounted. Therefore, the assumption of a small influence of flexibility effects cannot be applied to measurements obtained with the α vane. This result prompted further development regarding the FPR execution for this aircraft, aiming to obtain better results by using more adequate models.

It has been shown by [6] that an extension to the filter method used to reconstruct rigid body states, including the flexible body aircraft kinematics and additional sensors, can be effective. The developed Kalman filter was able to reconstruct the modal displacements and velocities of the studied aircraft, together with the traditional rigid body state variables. It was stated that the developed work is based on flexible aircraft kinematic equations and does not require a flight dynamics model, as long as displacement, rotation, and strain mode shapes are provided for the modes that are to be reconstructed.

This work aims to expand the FPR developed by [5] by applying a flexible aircraft model in the development of the FPR of the EOLO aircraft, still using the output error method (OEM).

2. EOLO UAV

The plane used in the study was a 4 m wingspan UAV named EOLO, built to be used as a test platform for flexible aircraft studies at the Aeronautics Institute of Technology (ITA). The aircraft is shown in Fig. 1, and Table 1 summarizes the main parameters of EOLO. Table 2 presents the modes obtained from the ground vibration tests of the EOLO UAV.



Figure 1 – Aircraft in the takeoff configuration [5].

Table 1 – EOLO UAV main characteristics [4]

Parameter	Value
Wing Area	0.85 m ²
Wing Chord	0.23 m
Wingspan	4.00 m
Wing Aspect Ratio	18.9
Total Length	1.89 m
Total Mass	9.4 kg

The aircraft control and data acquisition system is based on a flight computer developed by the aircraft manufacturing company. This computer receives the radio control inputs via a radio receiver, sends signals to actuate the servo motors of the flight controls, and has a telemetry link to a ground station. The computer relies on data acquired from an integrated inertial system, which provides accelerations and angular velocities, Euler angles, airspeed, barometric altitude, and GNSS data, among other information. Regarding the flexible aircraft studies, there is a secondary system to obtain measurements for the flexibility analysis. This secondary system communicates and receives data from the primary system while also obtaining data from an air data boom, used to measure the angle of attack (α) and angle of sideslip (β). In addition to those sensors, the aeroelastic acquisition system also has accelerometers and strain gauges, whose data can be used to identify the model, including the effects of the structural dynamics response during flight [5]. Figure 2 presents the

Table 2 – GVT obtained information for the first eight structural modes [7]

Mode	Freq. [Hz]	Damping [%]
1st symmetric wing bending	4.43	1.6
Tail-boom torsion	7.61	2.1
1st antisymmetric wing bending + tail-boom torsion	10.52	2.2
1st antisymmetric wing bending + tail-boom torsion	11.61	1.2
1st symmetric wing torsion + tail-boom bending	14.97	1.7
1st antisymmetric wing torsion	19.08	3.2
2nd symmetric wing bending + symmetric wing torsion	21.19	3.8
2nd antisymmetric wing bending	30.38	2.4

accelerometer and strain gauge sensor distribution on the aircraft. Figure 3 shows the α and β vanes on the right semi-wing.

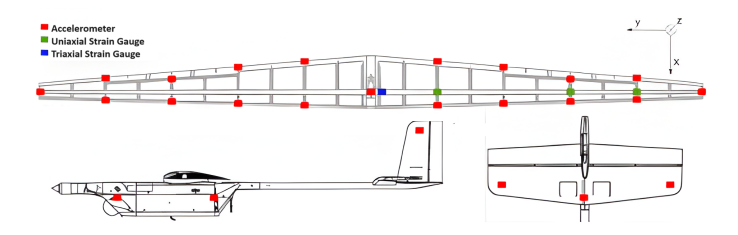


Figure 2 – Accelerometers and strain gauges position [8].



Figure 3 – α and β vanes [7].

3. Flight Path Reconstruction (FPR) - Rigid Body Kinematics

The work developed by [5] applied the rigid-body classical kinematics and OEM to develop an FPR for the EOLO UAV. This was based on [1] and relied on the assumption that the inertial measurement unit (IMU), which is integrated into the inertial system of the EOLO UAV, is mounted in a section with increased stiffness, not being highly influenced by the flexible structural dynamics. This hypothesis was also made by [3] for the SB10 glider and shown to be valid for this aircraft.

The development of the FPR relies on the physical formulation described below, involving the physical model of the aircraft, sensor observations, and correction equations. Eq. 1 presents a generic model described by [1] for modeling a sensor accounting for bias (Δy) , scale factor (K_y) , and time delay (τ) . The subscript c refers to the corrected value, while m refers to the recorded sensor data.

$$y_c(t) = K_v y_m(t - \tau) + \Delta y,\tag{1}$$

The kinematic equations described by [1] are presented in Eq. 2 and permit the determination of the state variables with the IMU data of the aircraft, not relying on aerodynamic coefficients and calculation of aerodynamic forces.

$$\dot{u} = -qw + rv - g\sin(\theta) + a_x^{CG},$$

$$\dot{v} = -ru + pw - g\cos(\theta)\sin(\phi) + a_y^{CG},$$

$$\dot{w} = -pv + qu - g\cos(\theta)\cos(\phi) + a_z^{CG},$$

$$\dot{\phi} = p + q\sin(\phi)\tan(\theta) + r\cos(\phi)\tan(\theta),$$

$$\dot{\theta} = q\cos(\theta) - r\sin(\phi),$$

$$\dot{\psi} = (q\sin(\phi) + r\cos(\phi))\sec(\theta),$$

$$\dot{h} = u\sin(\theta) - v\sin(\phi)\cos(\theta) - w\cos(\theta)\cos(\phi),$$
(2)

In Eq. 2, u, v, and w are the velocities in the aircraft body axes, the Euler angles ϕ and θ are the roll and pitch angles in the aircraft body axes, and h is the altitude. The yaw angle (ψ) , not present in the kinematics as the x and y positions are not being used, is described together with ϕ and θ in Eq. 3. The a_x^{CG} , a_y^{CG} , and a_z^{CG} are the linear accelerations at the center of gravity. The p, q, and r are the angular velocities and can be computed as described in Eq. 4.

$$\begin{split} \phi &= k_{\phi} \phi_{m} - \Delta \phi, \\ \theta &= k_{\theta} \theta_{m} - \Delta \theta, \\ \psi &= k_{\psi} \psi_{m} - \Delta \psi, \end{split} \tag{3}$$

$$p = k_p p_{IMU} - \Delta p,$$

$$q = k_q q_{IMU} - \Delta q,$$

$$r = k_r r_{IMU} - \Delta r,$$
(4)

As there are position offsets relative to the CG, they must be used in the FPR computations and are presented in Table 3 for the EOLO UAV instrumentation used in this work.

Table 3 – Position of sensors relative to the CG in the body axis [5, 7]

Sensor	x (m)	y (m)	z (m)
IMU	0.01	0.00	0.0120
Wingtip Accelerometer (L)	-0.0167	-2.00	-0.1122
Wingtip Accelerometer (R)	-0.0167	2.00	-0.1122
lpha Vane	0.120	0.400	-0.110
eta Vane	0.059	0.400	-0.110
Pitot tube	0.059	-0.400	-0.090

The calculation of the linear accelerations at the CG, accounting for the position offset of the IMU, the bias, and scale factors, can be done using Eq. 5. The time derivatives \dot{p} , \dot{q} , and \dot{r} are obtained from numerical differentiation of the angular rates.

$$a_{x}^{CG} = k_{ax} a_{x}^{IMU} + (q^{2} + r^{2}) x_{IMU} - (pq - \dot{r}) y_{IMU} - (pr + \dot{q}) z_{IMU} - \Delta a_{x},$$

$$a_{y}^{CG} = k_{ay} a_{y}^{IMU} - (pq + \dot{r}) x_{IMU} - (p^{2} + r^{2}) y_{IMU} - (qr - \dot{p}) z_{IMU} - \Delta a_{y},$$

$$a_{z}^{CG} = k_{az} a_{z}^{IMU} - (pr + \dot{q}) x_{IMU} - (qr + \dot{p}) y_{IMU} + (p^{2} + q^{2}) z_{IMU} - \Delta a_{z},$$
(5)

The computation of the local velocities at the pitot tube position can be done using Eq. 6. It is analogous for the u_{α} , v_{α} , w_{α} and u_{β} , v_{β} , w_{β} local velocities at the α and β vane positions, considering their respective offsets.

$$u_{pt} = u - ry_{pt} + qz_{pt},$$

 $v_{pt} = v - pz_{pt} + rx_{pt},$
 $w_{pt} = w - qx_{pt} + py_{pt},$
(6)

The observation values can be calculated as shown in Eq. 7. The subscript indicates a time shift in the variable, as stated in Eq. 1.

$$V_{m} = \sqrt{u^{2} + v^{2} + w^{2}},$$

$$\alpha_{m} = k_{\alpha} \arctan(w_{\alpha}/u_{\alpha})_{\tau_{\alpha}} + \Delta \alpha,$$

$$\beta_{m} = k_{\beta} \arcsin(v_{\beta}/\sqrt{u_{\beta}^{2} + v_{\beta}^{2} + w_{\beta}^{2}})_{\tau_{\beta}} + \Delta \beta,$$

$$\phi_{m} = k_{\phi} \phi_{\tau_{\phi}} - \Delta \phi,$$

$$\theta_{m} = k_{\theta} \theta_{\tau_{\theta}} - \Delta \theta,$$

$$\psi_{m} = k_{\psi} \psi_{\tau_{\psi}} - \Delta \psi,$$

$$h_{m} = h,$$

$$(7)$$

All the information about the FPR, states, observations, and parameters are presented in Tables 4 and 5.

Table 4 – Flight path reconstruction information [5]

Category	Variables	
States	$u, v, w, \phi, \theta, \psi, h$	
Inputs	$p_{IMU}, q_{IMU}, r_{IMU}, a_x^{IMU}, a_y^{IMU}, a_z^{IMU}$	
Observations	$V, \alpha, \beta, \phi, \theta, \psi, h$	

Table 5 – Flight Path Reconstruction Correction Parameters [5]

Category	Parameters
Biases	$\Delta a_x, \Delta a_y, \Delta a_z, \Delta p, \Delta q, \Delta r, \Delta \alpha, \Delta \beta, \Delta \phi, \Delta \theta, \Delta \psi$
Scale Factors	$k_{ax}, k_{ay}, k_{az}, k_p, k_q, k_r, k_{\alpha}, k_{\beta}, k_{\phi}, k_{\theta}, k_{\psi}$
Time Delays	$ au_{lpha}, au_{eta}, au_{\phi}, au_{eta}, au_{\psi}$

It was assumed that the α and β vanes were fixed in a section of the aircraft that does not experience deflections that could lead to significant influence of the flexible dynamics on the measurements, so those variables would be related only to the rigid body dynamics.

3.1 FPR - Rigid Body Kinematics - Results

The performed FPR using the rigid body kinematics, developed by [5], is shown in Fig. 5. It was constructed using nine flight segments with lateral-directional and longitudinal excitations. Fig. 4 shows the recorded data used as input for the FPR, except for \dot{p} , \dot{q} , and \dot{r} , which were obtained from numerical differentiation of the angular rates.

The results have shown a good fit for the reconstructed data for all attitude variables and also for the altitude. These variables are related to sensors that are located inside the aircraft fuselage, near the CG, and in a region with increased stiffness, which is in agreement with the assumption used in the application of rigid-body kinematics.

Airspeed and angle of attack values do not show as good a fit as the other variables. The sensors related to these measurements are not placed in an aircraft section with sufficient stiffness, as was initially considered. The mounting section of the α and β vanes is in the wing, and it is subjected to structural deformations during flight due to wing bending and torsion. The classical rigid body kinematics used does not account for these influences, which were initially thought to be minimal, based on the good results obtained by [3] for the SB 10 glider, shown in Fig. 6, which has its air data boom positioned similarly to the one in EOLO.

As concluded by [5], the results indicate the need to use a better-suited model, including corrections for the structural dynamics and angle of attack, as airspeed does show dependence on α and β .

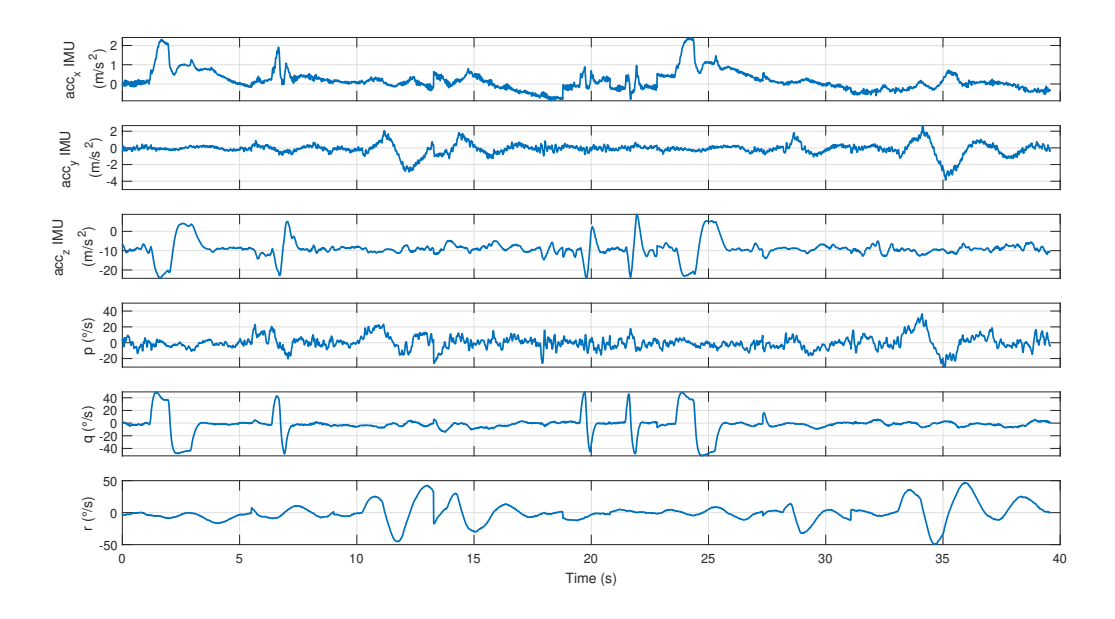


Figure 4 – FPR input data.

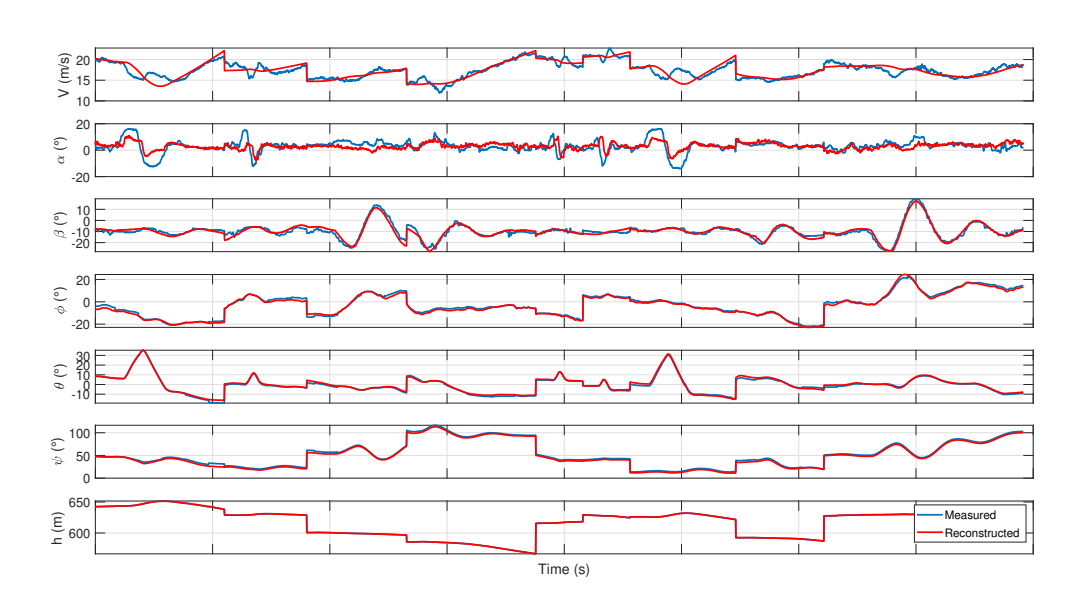


Figure 5 – FPR reconstructed data comparison with measured data [5].

4. Longitudinal Flight Path Reconstruction: Flexible Aircraft

To develop the necessary enhancements to the EOLO UAV FPR, the aircraft's structural model and its dynamics were considered in the reconstruction of the sensor outputs. The enhancements made to the FPR were restricted to the longitudinal dynamics for simplification.

It is important to state that the FPR developed for flexible aircraft differs from the rigid body FPR. The flexible FPR relies on data computed using the structural dynamics and the computation of loads using coefficients, which means that it is aircraft-dependent and also requires an a priori model, while the rigid body FPR only uses the kinematic model and the IMU data.

Therefore, additional equations and aircraft properties related to the structural dynamics are needed to account for the flexible aircraft. The sensor measurements that are influenced by the structural dynamics must have their responses adjusted, particularly for the variables that showed a mismatch in the rigid-body FPR. For this reason, the equations for airspeed and angle of attack must be enhanced to account for the structural deflections and velocities at the sensor positions. Additional

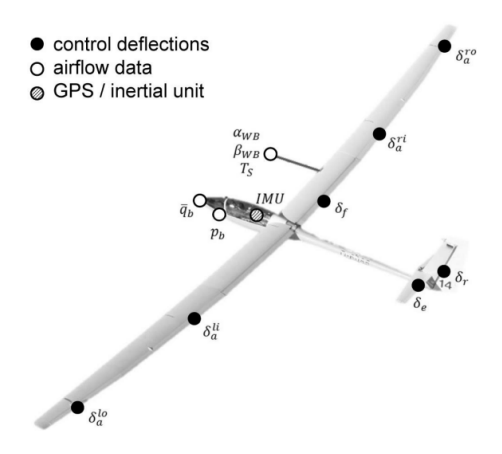


Figure 6 – Air data boom assembly on the SB 10 glider [3].

observation equations for accelerometers were also used, which permits further evaluation of the aircraft instrumentation and the proposed FPR.

The model proposed by [9] was used, as it reproduces the dynamics of a flexible aircraft. Eq. 8 presents the formulation for the structural dynamics considered in this study.

$$\ddot{\eta}_i + 2\xi_i \omega_i \dot{\eta}_i + \omega_i^2 \eta_i = \frac{Q_i}{m_i}, \quad i = 1, 2, 3, \dots, N$$
 (8)

In Eq. 8, the i term represents a structural mode. The η variable is the modal displacement, ω is the frequency, and ξ is the damping for a specific mode. The term Q_i represents the generalized load related to the i-th mode, and m_i is the modal mass of the mode. The expressions for obtaining Q_i are presented in [3] for an aircraft with complete dynamics (6 degrees of freedom, plus additional ones for the flexible modes). Eq. 9, Eq. 10, and Eq. 11 permit the computation of Q_i for an EOLO UAV model considering only the longitudinal dynamics.

$$Q_i = Q_{i_R} + Q_{i_F} \tag{9}$$

$$Q_{i_R} = \bar{q}S\bar{c}\left(C_0^{n_i} + C_\alpha^{n_i}\alpha + C_q^{n_i}\frac{q\bar{c}}{2V} + C_{\delta_e}^{n_i}\delta_e\right), \quad i = 1, 2, \dots, N$$

$$\tag{10}$$

$$Q_{i_F} = \bar{q} S \bar{c} \left(\sum_{j=1}^{N} C_{\eta_j}^{n_i} \eta_j + \sum_{j=1}^{N} C_{\dot{\eta}_j}^{n_i} \frac{\dot{\eta}_j l}{2V} \right), \quad i = 1, 2, \dots, N$$
(11)

In Eq. 10 and Eq. 11, \bar{q} is the dynamic pressure, \bar{c} is the mean aerodynamic chord, and S is the wing area. The terms $C_{\eta_j}^{n_i}\eta_j$ and $C_{\dot{\eta}_j}^{n_i}$ indicate the impact of the i-th modal deflection and its rate on the generalized load acting on the j-th mode, respectively. The term l is a reference length, and its value is the same as the mean aerodynamic chord (\bar{c}) for a symmetric structural mode [3].

Results obtained by [7] using GVT data provided by [4] were used to input the mode shapes, frequencies, and damping of each structural mode. The coefficients needed for the flexible dynamic model computations were obtained using the formulation presented in [9].

To compute the output of the aircraft sensors accounting for the structural dynamics, the formulations for accelerations in Eq. 12, rotations at sensor positions in Eq. 13, and velocities at other points of the structure formulated in Eq. 14 were used, as described in [3].

$$a_{x}^{k} = a_{x}^{CG} - x_{k}(q^{2} + r^{2}) + y_{k}(pq - \dot{r}) + z_{k}(pr + \dot{q}) + \sum_{i=1}^{N} \Phi_{x,n_{i}}^{k} \ddot{\eta}_{i},$$

$$a_{y}^{k} = a_{y}^{CG} + x_{k}(pq + \dot{r}) - y_{k}(p^{2} + r^{2}) + z_{k}(qr - \dot{p}) + \sum_{i=1}^{N} \Phi_{y,n_{i}}^{k} \ddot{\eta}_{i},$$

$$a_{z}^{k} = a_{z}^{CG} + x_{k}(pr - \dot{q}) + y_{k}(qr + \dot{p}) - z_{k}(p^{2} + q^{2}) + \sum_{i=1}^{N} \Phi_{z,n_{i}}^{k} \ddot{\eta}_{i}$$

$$(12)$$

$$v_x^k = \sum_{i=1}^N v_{x,n_i}^k \eta_i,$$

$$v_{y}^{k} = \sum_{i=1}^{N} v_{y,n_{i}}^{k} \eta_{i},$$

$$v_{z}^{k} = \sum_{i=1}^{N} v_{z,n_{i}}^{k} \eta_{i}.$$
(13)

$$p_{k} = p + \dot{v}_{x}^{k} = p + \sum_{i=1}^{N} v_{x,n_{i}}^{k} \ddot{\eta}_{i},$$

$$q_{k} = q + \dot{v}_{y}^{k} = q + \sum_{i=1}^{N} v_{y,n_{i}}^{k} \ddot{\eta}_{i},$$

$$r_{k} = r + \dot{v}_{z}^{k} = r + \sum_{i=1}^{N} v_{z,n_{i}}^{k} \ddot{\eta}_{i}.$$
(14)

In Eq. 12, the acceleration output of an accelerometer at a k position, distant x_k, y_k, z_k from the CG, is obtained. The terms $\Phi^k_{x,n_i}, \Phi^k_{y,n_i}$, and Φ^k_{z,n_i} are the mode shapes for each i mode considered, whose modal acceleration is $\ddot{\eta}_i$. In Eq. 13, η_i is the modal deformation, and v^k_{x,n_i} is the function of the rotation at that point for the i mode. Finally, in Eq. 14, the angular rates measured by a sensor at a k position are obtained [3].

Using the described formulations, a new FPR can be developed. The information for this FPR is presented in Table 6 and Table 7. In addition to the scale factors identified for the rigid model, new parameters k_{ACC_j} were introduced, where j corresponds to each new accelerometer considered. Bias parameters ΔACC_j were also added for each accelerometer. Finally, a new time delay τ_{ACC} was introduced to account for the time mismatch between the flexible aircraft data recorded and the rigid body data acquisition system, considering that the delay between each accelerometer for the flexible instrumentation was not significant.

Table 6 - Longitudinal Flight Path Reconstruction Information: Flexible Aircraft

Category	Variables
States	$u, w, \theta, h, \eta, \dot{\eta}$
Inputs	$q_{IMU}, \dot{q}_{IMU}, a_x^{IMU}, a_z^{IMU}$
Observations	$V^{Vane}, \pmb{lpha}^{Vane}, \pmb{ heta}, h, a_x^{ extstyle ilde{ heta}}, a_z^{ extstyle ilde{ heta}}$

4.1 Longitudinal Flight Path Reconstruction: Flexible Aircraft - Results

A simulation model was developed and used to generate synthetic data, capturing the aircraft's response to maneuvers that excited both structural and rigid body modes, allowing the development of the flexible FPR. The implemented model relies on the formulation proposed by [9] and is presented in [10].

Table 7 – Flight Path Reconstruction Correction Parameters - Flexible Aircraft - Longitudinal Dynamics

Category	Parameters
Biases	$\Delta a_x, \Delta a_z, \Delta q, \Delta \alpha, \Delta \theta, \Delta ACC_j$
Scale Factors	$k_{ax}, k_{az}, k_q, k_{\alpha}, k_{\theta}, k_{ACC_j}$
Time Delays	$ au_{lpha}, au_{oldsymbol{ heta}}, au_{ACC}$

Table 8 presents the dynamic modes information from this model, which was restricted to the longitudinal dynamics, including the first symmetric wing bending and first symmetric wing torsion structural degrees of freedom. In addition to the aircraft dynamic modes information, Table 8 also specifies the periods of 3211 maneuvers developed for the excitation of the rigid body and flexible modes, obtained according to [7].

Table 8 – Dynamic modes from the longitudinal flexible aircraft dynamics model

Pole	Damping	Frequency (Hz)	3211 maneuver period (s)
$-3.05 \pm 87.9i$	0.0347	14.0	0.0239
$-1.86 \pm 28.7i$	0.0645	4.57	0.0729
$-5.68 \pm 6.56i$	0.655	1.38	0.242
$-0.00906 \pm 0.531i$	0.0171	0.0845	3.95

The elevator deflection was used to excite the modes by applying 3211 maneuvers with 5 degrees of amplitude and the periods from Table 8. The input variables used to produce the results of the flexible FPR applied to the synthetically generated data are presented in Fig. 7 for the first three modes from Table 8.

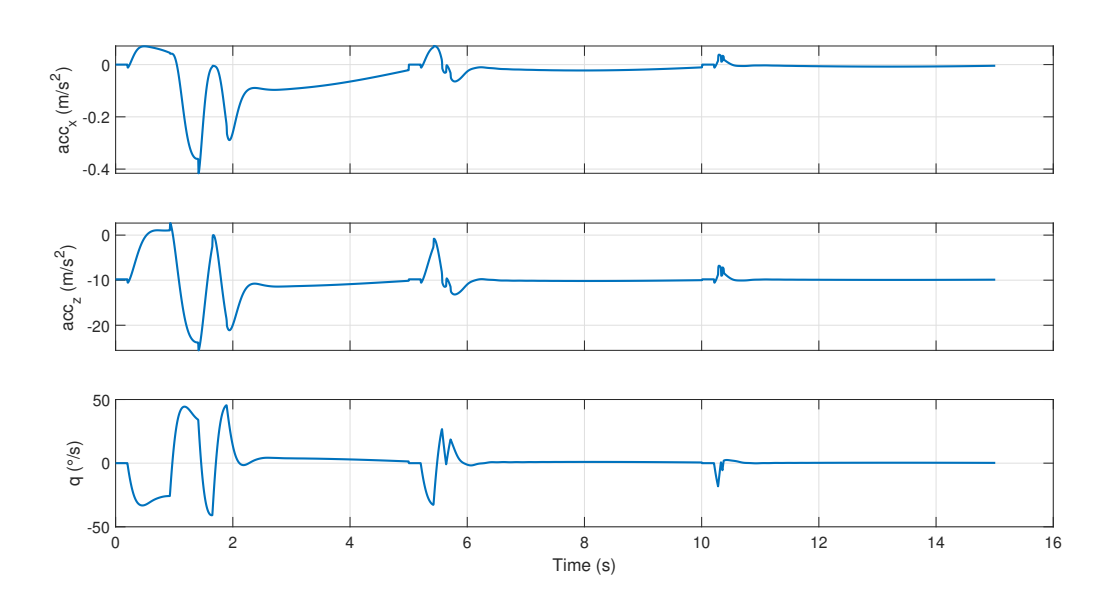


Figure 7 – Flexible FPR input variables for the EOLO UAV simulated data.

Fig. 8 shows the flexible FPR results obtained for the simulated data. The reconstruction of the output signals of the sensors and the simulated flight data shows a good agreement. Furthermore, the reconstructed signal of the wingtip accelerometer, which is highly dependent on the state variables η and its derivatives $\dot{\eta}$, was successfully obtained, demonstrating that these state variables can be derived from the FPR using the input variables from Table 4 and Eq. 8, together with the necessary derivatives for the computation of the term Q_i for each structural mode retained.

The results obtained from the synthetic data demonstrated the applicability of the flexible FPR, and the method was subsequently applied to data gathered from flights. The segments evaluated in

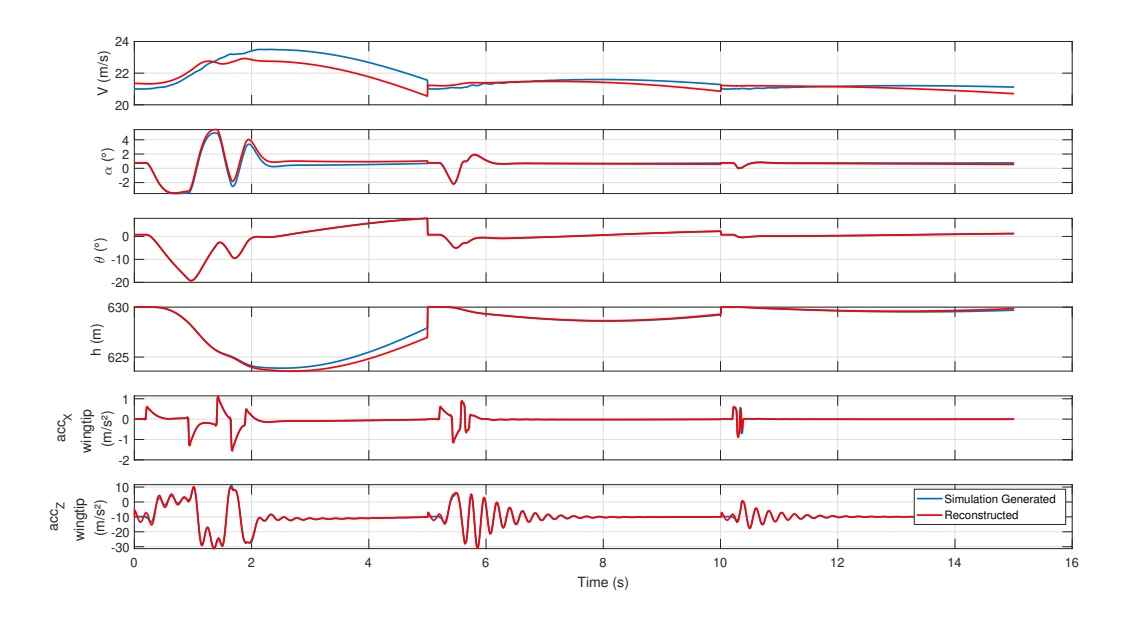


Figure 8 – Flexible FPR results for the EOLO UAV simulated data.

the execution of the classical FPR shown in Fig. 5 were initially considered, as they would permit a direct comparison of the results for the rigid body FPR and the flexible FPR. However, they were not adequate for use in the developed longitudinal flexible FPR.

Since the rigid FPR was conducted considering the complete aircraft dynamics, while the developed flexible FPR is restricted to longitudinal dynamics, the maneuvers using the rudder as input could not be used. Additionally, the maneuvers with elevator inputs were also inadequate for the isolated longitudinal study, as they presented high values of ϕ , which couples the longitudinal and lateral-directional dynamics.

Therefore, to apply the described strategy to the experimentally gathered data, a different segment, not used in the classical FPR shown in Fig. 5, was selected. The flight recorded input variables are presented in Fig. 9. The rigid-body FPR and its identified correction factors, developed by [5], were applied to this flight segment, and the results are shown in Fig. 10. The results are consistent with those from [5], as there is a good fit for the reconstructed attitude variables and altitude, but the airspeed and α show less agreement.

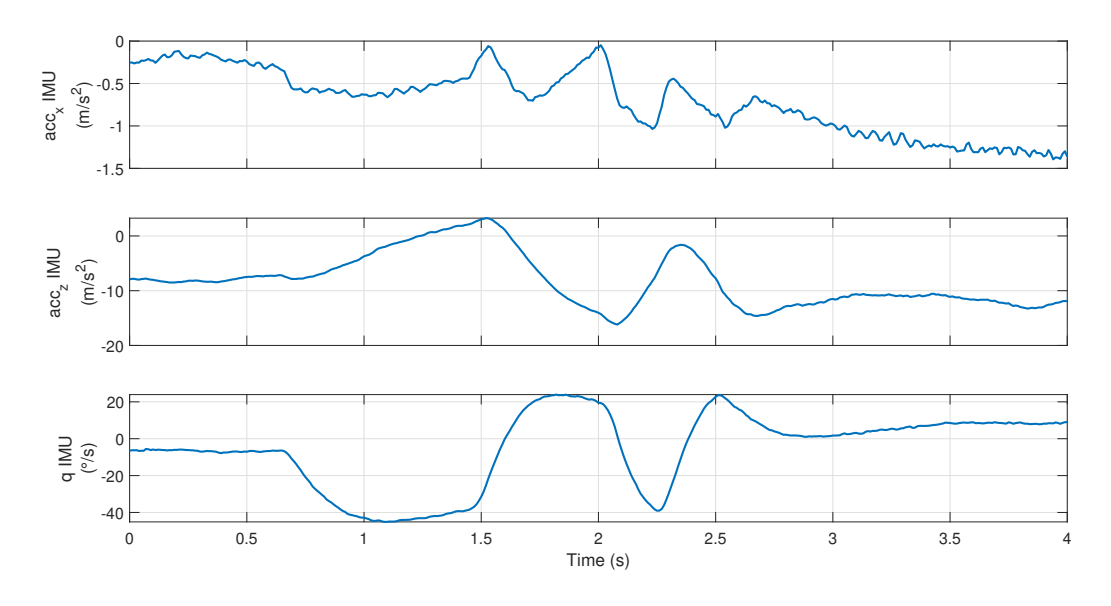


Figure 9 – Flight recorded input variables for the EOLO UAV rigid and flexible FPR.

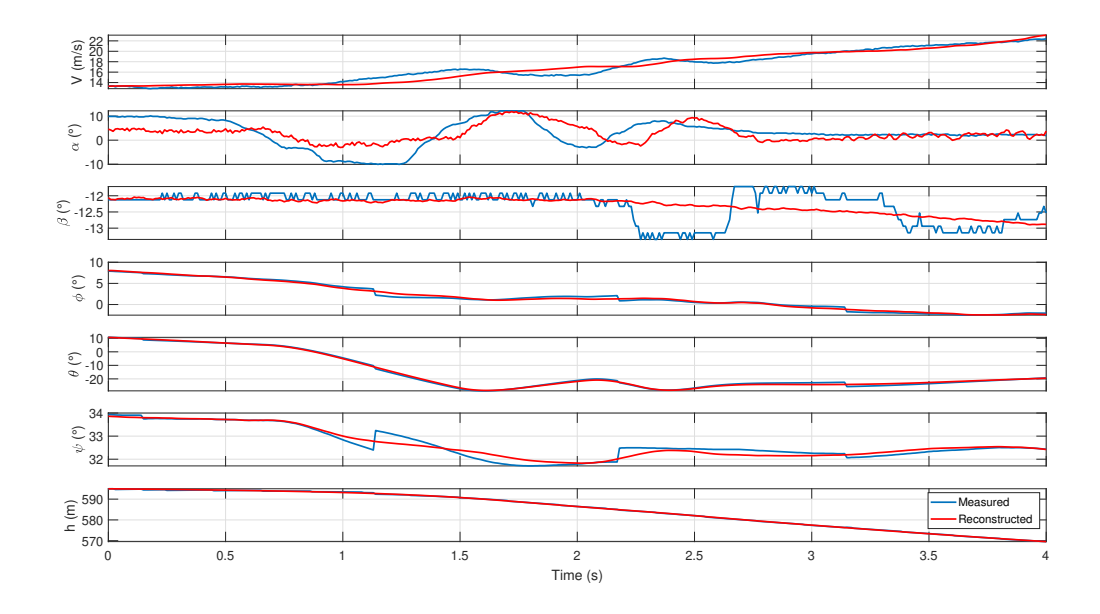


Figure 10 - Rigid-body FPR results for the EOLO UAV flight data.

The flexible FPR applied to the analyzed flight segment is presented in Fig. 11. In comparison with the rigid-body FPR, the airspeed results are similar, but an improvement can be seen in α . However, caution must be exercised, as the rigid-body FPR was developed using more segments, while the flexible FPR was applied only to this one. Increased concerns about the obtained results arise when evaluating the wingtip accelerations, which do not show a good fit. The accelerations in the X-axis do not reproduce the higher frequency oscillations present in the gathered data, capturing only the rigid body response. Furthermore, the flexible FPR was not able to reconstruct the output of the Z-axis acceleration sensor, which contrasts with the results from the simulated data, where the wingtip accelerations and reconstructed accelerometer outputs achieved a very good fit.

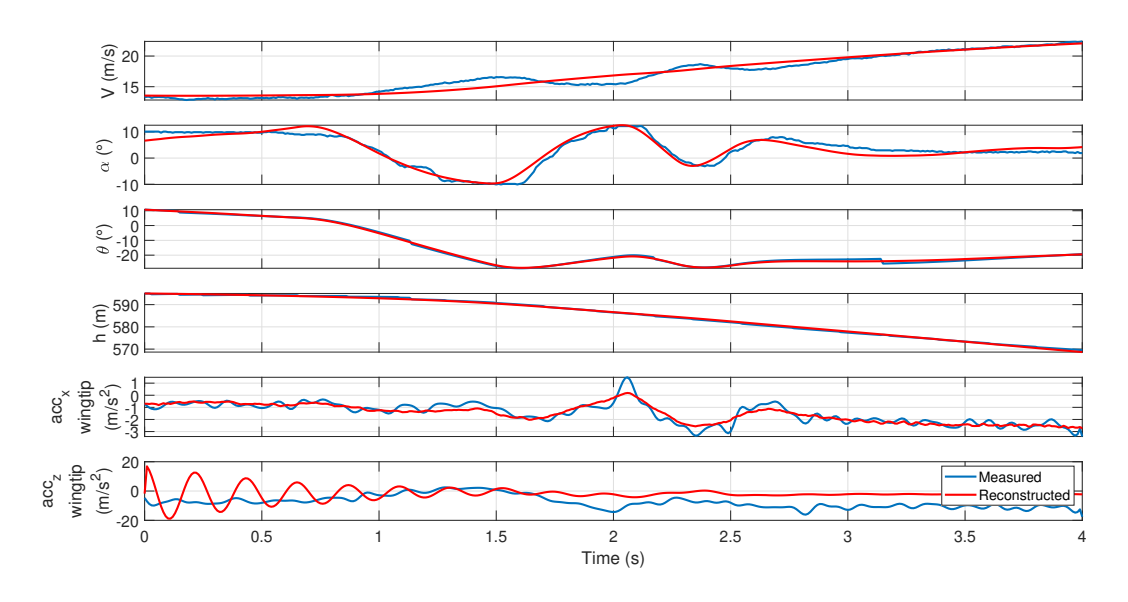


Figure 11 – Flexible FPR results for the EOLO UAV flight data.

The flexible FPR applied to the flight recorded data does not show a good agreement for all the observation variables. This could be related to the applied flexible aircraft model, aircraft instrumentation, or flight campaign execution. The results obtained in this work encourage the development of new flight campaigns to generate adequate input signals that excite all the desired modes while maintaining an appropriate aircraft attitude, without significant ϕ . Additionally, further performance

assessments of the data acquisition system are needed.

5. Conclusion

This study enhances the traditional Flight Path Reconstruction (FPR) methodology to better accommodate data from flexible aircraft by incorporating structural dynamics into the FPR process. The developed flexible FPR methodology was evaluated using synthetic data generated from a simulation of the EOLO UAV, demonstrating its capability to accurately reconstruct outputs from both traditional rigid-body sensors and wingtip accelerometers.

The results from the synthetic data validate the feasibility of the flexible FPR approach, showing good agreement between reconstructed and simulated sensor outputs. However, when applied to real flight data from the EOLO UAV, the flexible FPR did not yield significant improvements over the traditional rigid-body FPR. This discrepancy may be related to the quality of the sensor signals and the nature of the flight test campaign, which did not provide extensive data for the isolated evaluation of the longitudinal dynamics needed for the proposed FPR.

The findings suggest that further refinement of the data acquisition system and the development of new flight campaigns are necessary. Despite the challenges encountered with real flight data, the flexible FPR methodology holds promise for improving the accuracy of sensor data validation and system identification in flexible aircraft.

Future work will focus on conducting new flight test campaigns with optimized input signals, better initial conditions for the longitudinal maneuvers, and improved performance of the data acquisition system. These efforts aim to fully realize the potential of the flexible FPR methodology, contributing to more accurate and reliable flight data analysis.

6. Contact Author Email Address

mailto: vitor.paixao@ga.ita.br

7. Copyright Statement

The authors confirm that they, and/or their company or organization, hold copyright on all of the original material included in this paper. The authors also confirm that they have obtained permission, from the copyright holder of any third party material included in this paper, to publish it as part of their paper. The authors confirm that they give permission, or have obtained permission from the copyright holder of this paper, for the publication and distribution of this paper as part of the ICAS proceedings or as individual off-prints from the proceedings.

References

- [1] R. V. Jategaonkar. Flight Vehicle System Identification: A Time Domain Methodology. USA:AIAA, Reston, VA, 2015.
- [2] B. G. Silva and W. Monnich. System identification of flexible aircraft in time domain. *AIAA Atmospheric Flight Mechanics*, 2012.
- [3] B. G. O. Silva. *System Identification of Flexible Aircraft in Time Domain*. PhD thesis, DLR-Forschungsbericht, 2018.
- [4] David Fernando Castillo Zúñiga. *Aeroelastic Testing of Flexible Aircraft using Acceleration and Strain Sensors*. PhD thesis, Instituto Tecnológico de Aeronáutica, São José dos Campos, Brasil, 2019.
- [5] V. P. Fernandes, T. R. de Paula, R. C. Nascimento, L. C. S. Góes, R. G. A. Silva, and A. G. Souza. Flight campaign analysis of a flexible wing uav for studying flexible aircraft dynamics. *COBEM*, 2023.
- [6] Andres Jurisson, Bart Eussen, Coen C. de Visser, and Roeland De Breuker. *Flight path reconstruction filter extension for tracking flexible aircraft modal amplitudes and velocities.* 2023.
- [7] T. R. de Paula. Estudo do comportamento da dinâmica de voo de um vant flexível, 2023.
- [8] A. G. Souza, D. F. Castillo-Zúñiga, A. G. P. Sarmento, R. C. Machado, G. A. R. Silva, and L. C. S. Goes. Data compatibility check of an uas with a flexible wing. *DINAME*, XIX, 2023.
- [9] M. R. Waszak and D. K. Schmidt. Flight dynamics of aeroelastic vehicles. *Journal of Aircraft*, 25:563–571, 1988.
- [10] D.F. Castillo Zúñiga, A.G. Souza, and L.C.S. Góes. Flight dynamics modeling of a flexible wing unmanned aerial vehicle. *Mechanical Systems and Signal Processing*, 145:106900, 2020.